Supporting Information for:

Spectroscopic comparison of charge dynamics in fullerene and non-fullerene acceptor-based organic photovoltaic cells

Silvina N. Pugliese,[a b] Joseph K. Gallaher,[a,b b] Mohammad Afsar Uddin, Hwa Sook Ryu, Han Young Woo,[c] Justin M. Hodgkiss[a,b*]*

[a] School of Chemical and Physical Sciences, Victoria University of Wellington, New Zealand.

[b] MacDiarmid Institute for Advanced Materials and Nanotechnology, New Zealand.

[c] Department of Chemistry, Korea University, Seoul 136-713, Republic of Korea.

AUTHOR INFORMATION

Corresponding Author

* E-mail: Justin.Hodgkiss@vuw.ac.nz (J.M.H.), hywoo@korea.ac.kr (H.Y.W.)

Contents:

Experimental details

Optical spectroscopy sample preparation

PPDT2FBT:PCBM blend: A solution was made such that the polymer:fullerene (donor:acceptor) ratio was 1:1.5 (*w/w*) and the total concentration of donor + acceptor in chlorobenzene (CB) solution was 15 mg/ml. A volume fraction of 2% (by volume) of diphenlyether (DPE) additive was used. The solution was stirred at 80°C overnight before being spin-coated at 1000 rpm for 40 seconds onto a quartz substrate. Post thermal annealing treatment was performed at 70°C for 20 min on a heating plate.

PPDT2FBT:N2200 blend: A solution was made having a donor:acceptor ratio of 1:0.7 (*w/w*) and the total concentration of donor + acceptor in chloroform was 10 mg/ml. The volume fraction of diphenlyether (DPE) additive was 1 vol%. The solution was stirred at 45°C for one day before being spin-coated at 1000 rpm for 60 seconds onto a quartz substrate.

PPDT2FBT:NIDCS-HO blend: A solution was made having a donor:acceptor ratio of 1:2.5 (*w/w*) and the total concentration of donor + acceptor in chloroform was 10 mg/ml. The solution was stirred at 55°C overnight before being spin-coated at 1000 rpm for 60 seconds onto a quartz substrate. Post thermal annealing was performed at 90°C for 10min on a heating plate.

Optical spectroscopy measurements

Steady state UV-vis absorption spectra were collected using an Agilent 8453 UV-visible spectrophotometer over the range 220–1100 nm. All photophysical measurements were conducted on thin film samples cast on Spectrosil quartz substrates.

Transient absorption spectroscopy measurements were performed on samples under dynamic vacuum (10^{-5} mbar) using a homebuilt sample chamber. TA spectroscopy was carried out using an amplified Ti–sapphire laser (Spectra Physics, 100 fs pulse duration, 800 nm, 3 kHz). Pump pulses (excitation) were obtained by tuning a parametric amplifier (TOPAS) to the desired wavelength and using a retroreflector mounted in a mechanical delay stage to obtain pump-probe delays up to 6 ns. The excitation beam was attenuated to achieve a desired excitation intensity. Boradband probe pulses were generated by by focusing a small portion of output from the amplifier in a 3 mm YAG window. The spectral window of the broadband probe pulses covers the range 0.77-3.1 eV (equivalent to 400-1600 nm), allowing us to monitor dynamics of the photo-generated transient species. After transmission through the sample probe pulses were transmitted through a homebuilt prism based polymchromator and imaged on a linear Si photodiode array (visible wavelengths) and a linear InGaAs photodiode array (IR wavelengths). The differential transmission signal ($\Delta T/T$) is calculated using sequential probe shots corresponding to pump on vs. off. All transient absorption data was processed using MATLAB, such as background subtraction, wavelength calibration, and chirp correction.

MCR-ALS global fitting of TA spectroscopy

The individual contributions from excitons and charges to the overall TA signal were obtained by globally fitting the TA data matrix using soft-modelling analysis, namely, evolving factor analysis and model-free multivariate curve resolution alternating least squares (MCR-ALS) algorithm.[1,2] The number of components required was guided by performing singular value decomposition. Additionally, to address mathematical ambiguity we applied the following constraints: 1) that kinetic profiles cannot be negative, 2) the spectral signatures corresponding to the PIA region cannot be positive, and 3) using a spectral basis set comprising the spectrum

of a known excited state species (e.g., singlet excitons spectra determined using TA measurements on pristine polymers, or charges determined from long time signatures, as described in the text) as a spectral mask, i.e., a fixed spectra that is forced to match one of the MCR-ALS extracted components.

Global kinetic modelling of TA spectroscopy

The method implemented here to disentangle the temporal evolution of bound and separated polarons, named here as CT and SC, consists of using a model to describe the rate of change of these species, and optimise their profiles CT(t) and SC(t) such that the square of the residuals were minimised across measurements at different pump densities. The model is composed of vibrationally cold CT states which dissociate into SCs and SCs recombining non-geminately to the CT state, with all recombination to the ground state occurring via cold CT states at the donor-acceptor interfaces. This model is reminiscent of the Onsager-Braun model, and is described by the system of equations below, and a scheme is shown in Figure S1.

$$\frac{dCT(t)}{d(t)} = -k_d CT(t) - k_r CT(t) + \gamma SC(t)^{\lambda+1}$$

$$\frac{dSc(t)}{d(t)} = k_d CT(t) - \gamma SC(t)^{\lambda+1}$$

The Onsager-Braun model was developed by Braun to describe the charge generation process in donor:acceptor organic semiconductors, based on the Onsager theory for the dissociation and recombination of ions in solution.[3]. In this scenario, separated charges generated from the dissociation of CT states undergo transport (drift and diffusion) to either reach the collecting electrodes (desired process) or cancel out (recombine) when encountering an opposite charge

(undesired process). The yield of free carriers was specified by Braun as the product of the dissociation rate (k_d) and the lifetime of the CT states, i.e. the ratio of k_d and (k_d + k_r).[3] The main limitation of this model to describe the dissociation and recombination processes occurring in bulk-heterojunction OPVs is that the model assumes that carriers exist in a single phase, whereas holes and electrons in a bulk-heterojunction OPV live in different phases (holes in the donor phase and electrons in the acceptor phase).

The non-geminate recombination term in the kinetic model is described with a recombination constant γ and recombination order (γ+1), which is equal to two when the recombination process is bimolecular. Such recombination process is also analogous to the recombination of ions in solution, which can be described by the Langevin theory, where the recombination rate depends on the sum of electron and hole mobilities, and the recombination process is bimolecular. However, recombination orders in bulk-heterojunction OPV have been found to be higher than two. Different explanations for higher-order recombination include the trapping of charges in the tail states of the DOS and mobilities being charge carrier density dependent.

Since no analytical solution is found for CT(t) and SC(t) satisfying the equations of this kinetic model,[4] kinetic profiles are solved numerically assuming that all kinetic parameters are time independent. The best kinetic parameters are obtained by the simultaneous fit of the charge decay at different fluences. Prior to global fitting, TA charge signals were converted into charge densities using the cross-section value estimated for each blend, deduced from the Lambert-Beer law within the small signal approximation:

$$\frac{\Delta T}{T} = -\sigma N d$$

where σ is the cross-section of the electronic transition (in cm^2), N is the charge density (in cm^{-3}) and d is the film thickness (in cm).

In principle, the best kinetic parameters can be obtained by ordinary least-squares, minimising the sum of the squares of the residuals between the data and the model, with guess initial values and bounds on the variables. However, we found that the output parameters are sensitive to the choice of the initial values, indicating the presence of several local minima. To avoid this problem, global optimization was achieved by applying the differential evolution algorithm by Storn and Price,[5] from the Python library scipy.optimize. Our code allows us to fix parameters in the model to static values, for example, we can set the recombination order to a value of two, to evaluate the fitting outputs considering nongeminate recombination as a bimolecular process.

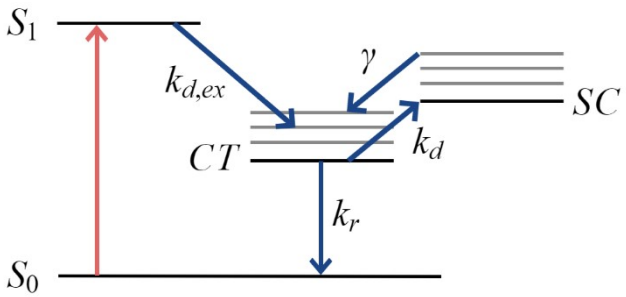

Figure S1. Scheme of the kinetic model described by the equations above, and description in the text.

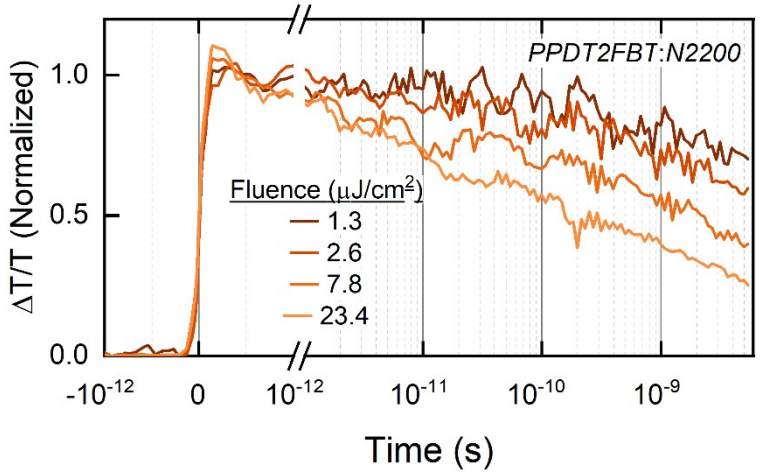

Figure S2. Intensity dependent recombination for the PPDT2FBT:N2200 blend at the fluences indicated in the legend entries. Excitation wavelength was 532 nm.

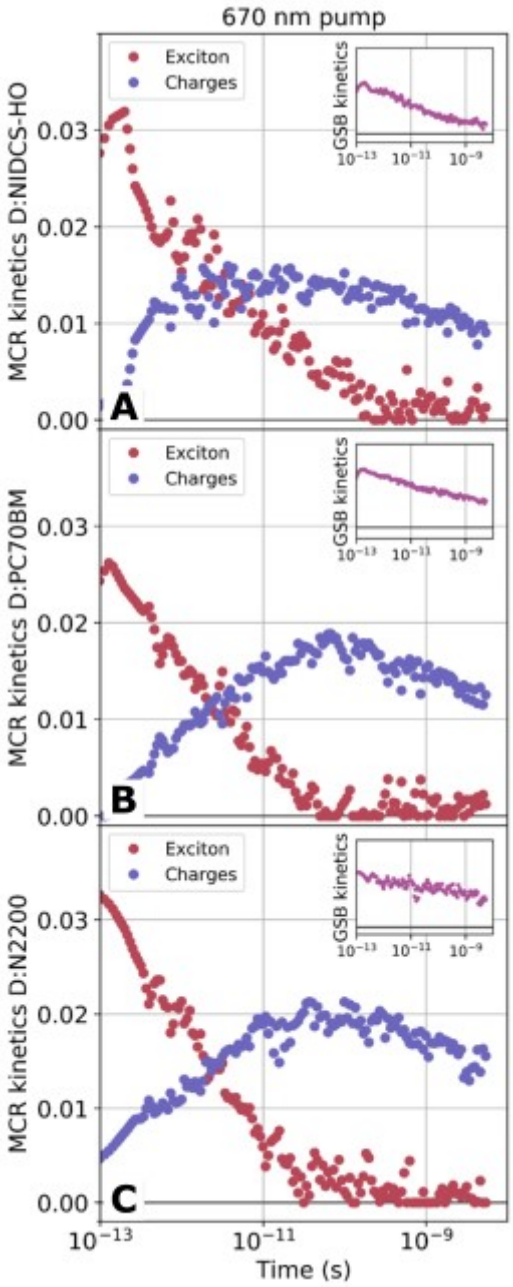

Figure S3. MCR kinetics and insets showing the integrated GSB kinetics for A) PPDT2FBT:NIDCS-HO, B) PPDT2FBT:PCBM, and C) PPDT2FBT:N2200 using 670 nm excitation wavelength.

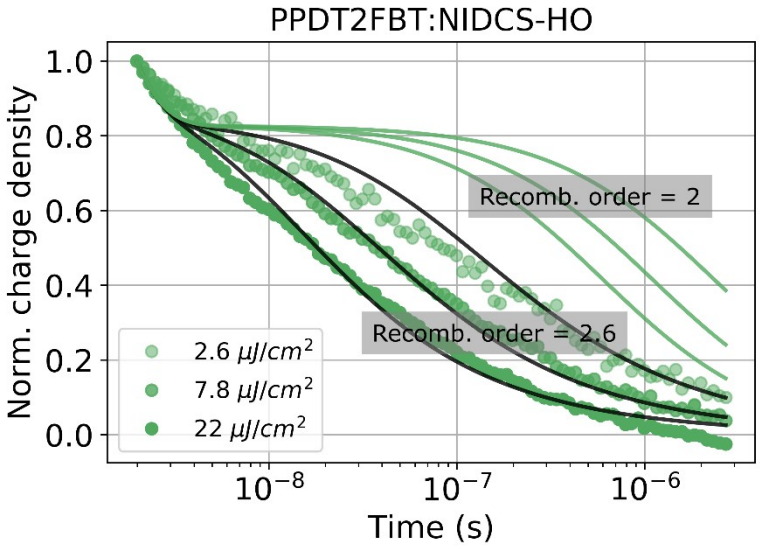

Figure S3: Global fitting curves for PPDT2FBT:NIDCS-HO where the kinetic constants were fixed and the recombination order was changed to a value of 2.

References:

1. Jaumot, J.; de Juan, A.; Tauler, R. MCR-ALS GUI 2.0: New Features and Applications. Chemom. Intell. Lab. Syst. 2015, 140, 1–12.
2. Jaumot, J.; Gargallo, R.; De Juan, A.; Tauler, R. A Graphical User-Friendly Interface for MCR-ALS: A New Tool for Multivariate Curve Resolution in MATLAB. Chemom. Intell. Lab. Syst. 2005, 76 (1), 101–110.
3. (Shoaee, S.; Stolterfoht, M.; Neher, D. The Role of Mobility on Charge Generation, Recombination, and Extraction in Polymer-Based Solar Cells. Adv. Energy Mater. 2018, 8 (28), 1–20.
4. Howard, I. A.; Mauer, R.; Meister, M.; Laquai, F. Effect of Morphology on Ultrafast Free Carrier Generation in Polythiophene:Fullerene Organic Solar Cells. J. Am. Chem. Soc. 2010, 132 (42), 14866–14876.
5. Storn, R.; Price, K. Differential Evolution – A Simple and Efficient Heuristic for Global Optimization over Continuous Spaces. J. Glob. Optim. 1997, 11 (4), 341–359.